SIMULATION OF MICROSTRUCTURAL EVOLUTION OF CROSS-LINKED TEMPLATED SILICA-AEROGELS UNDER COMPRESSION

By

BOSHEN FU

Bachelor of Science in Mechanical Design Manufacture

& Automation

East China University of Science and Technology

Shanghai, P. R. China

2003

Submitted to the Faculty of the
Graduate College of the
Oklahoma State University
in partial fulfillment of
the requirements for
the Degree of
MASTER OF SCIENCE
December, 2009

SIMULATION OF MICROSTRUCTURAL EVOLUTION

OF CROSS-LINKED TEMPLATED SILICA-AEROGELS

UNDER COMPRESSION

Thesis Approved:

Dr. Hongbing Lu

Thesis Adviser

Dr. Jay Hanan

Dr. Ronald Delahoussaye

Dr. A. Gordon Emslie

Dean of the Graduate College

ACKNOWLEDGMENTS

First of all, I would like to take this opportunity to thank my advisor Dr. Hongbing Lu for his immense support and guidance during this study; working with him is a great opportunity and honor. I would also like to appreciate the guidance of other faculty members in my master degree assessment committee, Drs. Jay Hanan and Ronald Delahoussaye. All of them have played vital roles in different aspects of this work.

We acknowledge the support of NSF under CMMI-0653919 & CMMI-0653970. We also thank the support of AFOSR DEPSCoR FA955-05-1-0481 for the setup of the SHPB and the oscilloscope, as well as NSF CMS-0320968 for the acquisition of the ultra-high speed camera. The author would like to thank support from Drs. Sotiriou-Leventis and Leventis for providing aerogel preparation technique, Dr. Huiyang Luo for providing SHPB experimental results and Dr. Dana Brunson for supplying the parallel computational cluster. Acknowledgements are due to Drs. Jin Ma and Nitin Daphalapurkar for providing the parallel versions of MPM codes and helpful discussions; Mr. Hrishikesh Bale for assistance with post-processing of simulation output. We thank TeraGrid for the technical support on the parallel processing, and thank Mr. Gitogo Churu for preparing the X-MP4-T045 samples for experiments. I would like to acknowledge helpful discussions on SAMRAI with Dr. Kevin Chu. Finally I eternally appreciate to my parents for their motivation and lovely concern all the time. I am also deeply grateful to my wife, Fang, for her support and patience of my work.

TABLE OF CONTENTS

LIST OF FIGURES

Figure Page

Figure Page

CHAPTER I

INTRODUCTION

Silica-aerogels are ultra-low-density assemblies of silica nanoparticles, and possess practically useful material properties, such as high acoustic impedance (e.g., the sound wave speed is less than 100 m/s) (Fricke, 1992) and extremely low thermal conductivity (less than 20 $mWm^{-1}K^{-1}$) (Pierre *et al*., 2002). Silica-aerogels have been considered for use in many applications, for instance, in thermal insulating, as Cerenkov radiation detectors, and capturing cosmic dust particles (Jones, 2006, Fricke, 1992, Pierre *et al*., 2002, Tsou, 1995), however, their fragile material properties limited their commercial use. In order to increase the strength of aerogels, Leventis *et al.* (2002 & 2007) invented a new class of polymer nanoencapsulated aerogels with exceptional mechanical properties. Those polymer cross-linked aerogels are obtained by nano encapsulating the aerogel skeletal framework using a polymer coating (Leventis, 2007). The polymer coating reinforces the inter particle necks and increases the ultimate compressive strength of the material dramatically (Leventis *et al*., 2008) without clogging the pores of aerogels. Manufacturing of such cross-linked silica-aerogel structures, depending on the type and shape of the nanoparticles, the polymer cross-linker and the chemistry in use, yields structures with vastly different morphologies and a wide range of mechanical properties. In this context, in order to optimize the structure-properties

relationship it has become necessary to understand the microstructure-macroscopic property relationship and develop a predictive method for the mechanical performance.

Therefore there is a need for modeling of the silica-aerogel material properties via a mesoscale and up approach. Such methodology has not been considered by the current phenomenological models for aerogels which are based on the continuum material assumption. Work on the simulations of the relationship between nano/microstructure and mechanical property of aerogels is very limited. The previous work was primarily on generation of mesoporous silica aerogel structure using the Diffusion-Limited Cluster-Cluster Aggregation (Roberts, 1997; Primera *et al.*, 2005), and the simulation of mechanical behavior such as fracture behavior using molecular statics-based numerical method (Good, 2006). The simulations for microstructural evolution and mechanical response under compression of porous materials like silica-aerogel have not yet been reported. In this work, we use a relatively new numerical method, namely the Material Point Method (MPM) (Sulsky *et al*., 1995) to simulate the compression of polymer cross-linked template silica aerogels. Details on MPM will be given in next section. MPM has already been used effectively in modeling the microstructural evolution of the polymethacrylimide (PMI) closed-cell plastic foam (Rohacell foam) with 70% porosity (Daphalapurkar *et al.*, 2008), where 3D X-ray micro-tomograph was used to reconstruct the microstructure of PMI plastic foam for use in simulations. PMI plastic foam is not an aerogel due to its low surface area; it is, however, porous, a common feature with aerogels, consequently, MPM should be also a very suitable method for simulation of the evolution of porous nanostructure of silica-aerogels. In this aspect, an approach based on the model generated from X-ray nano-computed tomography (n-CT) is used to obtain and

construct a model of the microstructure of cross-linked silica-aerogels. The voxel information from the tomography is used to generate material points in MPM. A parallel MPM code using the Structured Adaptive Mesh Refinement Application Infrastructure (Hornung *et al.*, 2002) is used to simulate the mechanical response and microstructural evolution of the silica-aerogel model under compression. Because the MPM is developed based on dynamic (explicit) method, the results from the simulation of a cross-linked templated silica-aerogel (X-MP4-T045) under compression are compared with the compressive stress-strain curve obtained from dynamic experiments using a long split Hopkinson pressure bar (SHPB). While Luo *et al.* (2006 & 2008) reported the compressive behavior of some cross-linked silica and vandia aerogels at high strain rates. Results on the stress-strain relationship of cross-linked template silica-aerogels, namely X-MP4-T045 (Luo *et al.*, 2008) used in this work were not reported; they were measured in this work using the approach described in Luo *et al.* (2006) for use in comparison with simulation results. Similarly to mechanical response of other porous materials' under compression, the evolution of the silica-aerogel deformation shows three stages: an elastic deformation region at small strain levels; when the stains reach to the certain level, pores are compacted, which causes a plastic hardening in the stress-strain curves; finally, the densification region.

Previous work (Leventis *et al*., 2007 & 2008) shows there are three degrees of freedom in the design space of cross-linked aerogels: the nanoparticles surface chemistry, the chemical identity of the cross-linking and the network morphology. Here we focus on the function of the polymer coating and the effect of the microstructure, as means to improve the design of cross-linked aerogel. It is known that polymer coating around

skeletal silica particles enhances the mechanical properties of silica-aerogels. To explore the function of the polymer coating, different porosity models with and without a polymer coating are employed in the simulations. In previous work (Woignier *et al.*, 1987 & 1989) on the mechanical properties of silica-aerogels, power law relationships has been indentified between such properties, (e.g. the Young's Modulus and the aerogel densities ρ). Using the simulation results from this work, we investigated the dependence of mechanical properties on the porosity of cross-linked templated silica-aerogels. Scherer *et al.* (1995) have established a relationship between modulus and density (porosity), and they evaluated the method by using the relation between bulk modulus, *K*, and the volumetric deformation, and reported the parameters of the power law function at a small strain level and at the plastic strain level to be 3.6 and ~ 3.2, respectively. Here we discuss this power law relationship between the stress response and densities of silica-aerogel through MPM simulations, and investigate the effect of microstructure on the power law relationship.

CHAPTER II

MATERIAL POINT METHOD (MPM)

2.1 Background

The material point method was used to model cross-linked templated silica-aerogels under compression, and it is introduced here briefly for completeness of presentation. MPM evolved from the Particle-in-Cell (PIC) method (Harlow, 1964; Brackbill, *et al.,* 1986 & 1988) and it was first formulated for simulation of solid mechanics problems by Sulsky *et al.* (1995). Further developments have been made since then (e.g, Bardenhagen *et al.,* 2000; Tan and Narin, 2002; Wang *et al.,* 2005). Bardenhagen and Kober (2004) introduced C^1 continuous interpolation functions in order to resolve the instability problems in MPM simulation. Structured mesh refinement has been introduced for adaptive material points (Ma *et al.* 2005). Irregular background mesh was introduced in MPM to simulate problems such as crack propagation (Wang *et al.*, 2005) using adaptive background mesh. MPM gives the same results as finite element method (Ma *et al.* 2005 & 2006, Wang *et al.,* 2005) but can simulate complex structures involving large deformation and complex surface contacts (Bardenhagen *et al*., 2005, Daphalapurkar *et al.*, 2006 & 2008).

2.2 Numerical methodology

In MPM, the material continuum is discretized into finite material volumes in

3D (or areas in 2D). Each material point is assigned a mass consistent with the material density and volume of the point, and all of variables used in the simulation, such as position, velocity, acceleration, stress, and strain. Physical variables carried by the material points are projected to the background computational grid using shape functions, the governing equations are solved at the background gird and the states of the physical variables are updated based on the calculation. For simulations of dynamic problems, the equations of motion are conservation mass and momentum equations

$$\frac{\mathrm{d}\rho}{\mathrm{d}t} + \rho\nabla \cdot \mathbf{v} = 0, \tag{1}$$

$$\rho\mathbf{a} = \nabla \cdot \boldsymbol{\sigma} + \mathbf{b}, \tag{2}$$

where ρ is the material mass density, $\mathbf{a}$ is the acceleration vector, $\boldsymbol{\sigma}$ is the Cauchy stress tensor and $\mathbf{b}$ is the body force density vector. The displacement and traction boundary conditions are

$$\mathbf{u} = \bar{\mathbf{u}} \text{ on } \partial\Omega_{\mathrm{u}}, \tag{3}$$

$$\tau = \bar{\tau} \text{ on } \partial\Omega_{\tau}, \tag{4}$$

where $\partial\Omega_{\mathrm{u}} \cap \partial\Omega_{\tau} = \emptyset$, and $\partial\Omega = \partial\Omega_{\mathrm{u}} \cap \partial\Omega_{\tau}$. The equation of motion can be written as variational form

$$\int_{\Omega} \rho\mathbf{a} \cdot \delta\mathbf{v}\, \mathrm{d}\mathbf{x} = \int_{\Omega} (\nabla \cdot \boldsymbol{\sigma}) \cdot \delta\mathbf{v}\, \mathrm{d}\mathbf{x} + \int_{\Omega} \mathbf{b} \cdot \delta\mathbf{v}\, \mathrm{d}\mathbf{x}, \tag{5}$$

where $\delta\mathbf{v}$ is an admissible velocity field. Applying the chain rule and divergence theorem, equation (5) is written as

$$\int_{\Omega} \rho\mathbf{a} \cdot \delta\mathbf{v}\, \mathrm{d}\mathbf{x} + \int_{\Omega} \boldsymbol{\sigma} : \nabla\delta\mathbf{v}\, \mathrm{d}\mathbf{x} = \int_{\Omega} \rho\mathbf{b} \cdot \delta\mathbf{v}\, \mathrm{d}\mathbf{x} + \int_{\partial\Omega_{\tau}} \boldsymbol{\tau} \cdot \delta\mathbf{v}\, \mathrm{d}\mathbf{x}. \tag{6}$$

In MPM, the discretization procedure is to use a collection of material particles to represent a solid continuum, and the domain of particle p represented by $\partial\Omega_{\mathrm{p}}$. The

particle characteristic functions $\chi_p(\mathbf{x})$, are used to define the particles (Bardenhagen *et al.*, 2004), the initial configuration is

$$\sum_p \chi_p^i(\mathbf{x}) = 1 \quad \forall \mathbf{x}. \tag{7}$$

Physical variables of the particles, such as volume, mass, stress and momentum can be calculated. For instance, the volume, mass, and momentum for particle p can be calculated as:

$$V_p^i = \int_{\Omega^i} \chi_p^i(\mathbf{x}) \mathrm{d}\,\mathbf{x}, \tag{8}$$

$$m_p^i = \int_{\Omega^i} \rho^i(\mathbf{x}) \chi_p^i(\mathbf{x}) \mathrm{d}\,\mathbf{x}, \tag{9}$$

$$\mathbf{P}_p^i = \int_{\Omega^i} \rho^i(\mathbf{x}) \mathbf{v}^i(\mathbf{x}) \chi_p^i(\mathbf{x}) \mathrm{d}\,\mathbf{x}, \tag{10}$$

where Ω^i is the initial volume of the discretized body. Using equation (7), the equation (9) and equation (10) may be written as:

$$\sum_p m_p^i = \sum_p \int_{\Omega^i} \rho^i(\mathbf{x}) \chi_p^i(\mathbf{x}) \mathrm{d}\,\mathbf{x} = \int_{\Omega^i} \rho^i(\mathbf{x}) \mathrm{d}\,\mathbf{x}, \tag{11}$$

$$\sum_p \mathbf{P}_p^i = \sum_p \int_{\Omega^i} \rho^i(\mathbf{x}) \mathbf{v}^i(\mathbf{x}) \chi_p^i(\mathbf{x}) \mathrm{d}\,\mathbf{x} = \int_{\Omega^i} \rho^i(\mathbf{x}) \mathbf{v}^i(\mathbf{x}) \mathrm{d}\,\mathbf{x} \tag{12}$$

Thus the equation of motion over particles is discretized as

$$\sum_p \int_{\Omega \cap \Omega_p} \frac{\dot{\mathbf{P}}_p \chi_p}{V_p} \cdot \delta\mathbf{v} \mathrm{d}\mathbf{x} + \sum_p \int_{\Omega \cap \Omega_p} \boldsymbol{\sigma}_p \chi_p : \delta\mathbf{v} \mathrm{d}\mathbf{x} = \sum_p \int_{\Omega \cap \Omega_p} \frac{m_p \chi_p}{V_p} \mathbf{b} \cdot \delta\mathbf{v} \mathrm{d}\mathbf{x} + \sum_p \int_{\partial\Omega_p} \boldsymbol{\tau} \cdot \delta\mathbf{v} \mathrm{d}\mathbf{x}, \tag{13}$$

where m_p is the lumped mass of each particle. In MPM, the information carried by particle is updated from the solution of the equation of motion. A computational grid shape function $S_i(\mathbf{x})$, is introduced to project physical variables from material points to background grid and vice versa. The grid shape function satisfies the partition of unity

$\sum_i S_i(\mathbf{x}) = 1$. Using the grid shape function, the admissible velocity can be computed from the gird nodal data. The discrete equation of motion for each node i is

$$\dot{\mathbf{P}}_i = \mathbf{f}_i^{int} + \mathbf{f}_i^{b} + \mathbf{f}_i^{\tau}, \tag{14}$$

where,

$$\dot{\mathbf{P}}_i = \sum_p \bar{S}_{ip} \frac{\mathbf{P}_p}{\Delta t}, \tag{15}$$

$$\mathbf{f}_i^{int} = -\sum_p \sigma_p \cdot \overline{\nabla S}_{ip} V_p, \tag{16}$$

$$\mathbf{f}_i^{b} = \sum_p m_p \mathbf{b} \bar{S}_{ip}, \tag{17}$$

$$\mathbf{f}_i^{\tau} = \sum_p \int_{\partial\Omega_\tau \cap \Omega_p} \bar{\boldsymbol{\tau}} S_i(\mathbf{x}) dS, \tag{18}$$

$\bar{S}_{ip}$ and $\overline{\nabla S}_{ip}$ are weighting function and gradient weighting function, respectively, between the particle p and the grid node i. In this work, we use a C^1 continuous weighting function as given by Bardenhagen & Kober (2000)

$$\bar{S}_{vp} = \frac{1}{V_p} \int_{\Omega_p \cap \Omega} \chi_p(\mathbf{x}) S_i(\mathbf{x}) d\mathbf{x}, \tag{19}$$

$$\overline{\nabla S}_{vp} = \frac{1}{V_p} \int_{\Omega_p \cap \Omega} \chi_p(\mathbf{x}) \nabla S_i(\mathbf{x}) d\mathbf{x}. \tag{20}$$

The equation of motion is solved at each node to update the nodal momentum, acceleration, and velocity. These updated nodal variables are then projected to the material points to update the particle position, velocity, stress, and strain. For material the constitutive relation is

$$\boldsymbol{\sigma} = \mathbf{C} : \boldsymbol{\varepsilon}, \tag{21}$$

where $\boldsymbol{C}$ is a fourth order elasticity tensor.

CHAPTER III

PREPARATION OF CROSS-LINKED TEMPLATED SILICA-AEROGEL SAMPLES

The material simulated was what is referred to as X-MP4-T045 (Nakanishi, 1997; Leventis *et al*., 2007 & 2008), and it was prepared in this work. In a typical preparation procedure, 4.0 g of Pluronic P123 was dissolved in 12 g of a 1.0 M aqueous solution of nitric acid, and the desired amount of TMB was added under magnetic stirring at room temperature. After 30 minutes the samples were cooled down to 0° C and all kept there for 30 minutes; subsequently 5.15 g of TMOS was added to the solution under vigorous stirring. After stirred for an additional 10 minutes, the samples were poured into molds. The molds were then sealed and placed in a 60 °C oven for gelation. The resulting wet gels were aged in their molds at 60 °C for five times of their gelation time. At the end of that period, all wet gels were immersed into ethanol and washed by ethanol twice in 8 hrs intervals, and then to remove P123 soxhlet extraction using CH_3CN as solvent. The gels then were put into pure dry acetone and washed. Subsequently, gels were placed into a solution containing Desmodur N3200 of acetone solution, and were kept in that solution at room temperature for 24 hrs. Then the sample with the N3200 solution was heated at 55 °C for three days. After three days heating, the samples will be placed into acetone and they were washed 4× at 8 hr interval, in pentane and drying from pentane at 40 °C under ambient pressure to obtain cross-linked silica-aerogel (X-MP4-T045). Using

Nakanishi's notation (Nakanishi, 1997) in the standard formulation, "M" stands for Mesoporous, "P4" refers to 4 grams of the templating agent (Pluronic P123) used and "T045" refers to the specific amount of the swelling agent (trimethylbenzene) used. That formulation yields macroporous structures consisting of micron-sized worm objects, which in turn are perforated with mesoporous tubes. "X" signifies that the MP4-T045 microstructure has been cross-linked with polymer. The detail procedure was well documented in Leventis *et al*. (2007 & 2008).

CHAPTER IV

SIMULATION OF MICROSTRUCTURAL EVOLUTION OF CROSS-LINKED TEMPLATED SILICA-AEROGELS UNDER COMPRESSION

4.1 Nano-computerized tomography (n-CT) and 3D model reconstruction

To generate the model for the MPM simulation, the nanostructure was obtained using an X-ray nanotomography apparatus (or n-CT, SkyScan 2011, Micro Photonics Inc.). During each scanning step, X-rays with an initial intensity I_0 pass through a specimen. As the sample absorbs part of the energy, the incident intensity of the X-ray is attenuated to *I*. A scintillator converts the X-ray to visible light, which is recorded by a CCD camera. X-ray images were obtained at quarter degree increments from 0º to 180º and they are radiographs. All radiographs are analyzed to reconstruct a series of 2D images representing the local density of the material. Figure 4.1 shows n-CT 3D reconstruction model and the Scanning Electron Micrographs (SEM) image. The n-CT tomographic images are used to generate the 3D MPM model. The SEM images and n-CT images indicate nearly identical microstructure for the silica-aerogel. Based on this observation, it was reasonable to use n-CT for the construction of the 3D model for MPM simulation.

Each voxel in an n-CT tomograph is 480×480×480 nm^3; it was converted to a 3D material point in MPM simulations. The porosity of X-MP4-T045 is 50%, measured

using nitrogen sorption, and in this simulation we obtained the model with 50% porosity by controlling the grayscale of the n-CT images when we reconstructed the 3D model. The cut-off grayscale value that is able to produce a 50% porosity model is 58. The model which will be employed in MPM simulation using different cut-off grayscale value is also shown in Figure 4.2. For conducting simulations at different porosities, we found that there is a linear relationship between the cut-off grayscale of the images and the porosity of the sample (Figure 4.2). Two different model sizes, 100×100×100 voxels and 200×200×200 voxels (representing 48×48×48 μm^3 cube and 96×96×96 μm^3 cube respectively), are considered for finding the relationship as shown in Figure 4.2, and both show that the porosity decreases when the cut-off grayscale increases, which agrees with a linear relationship. In n-CT scanning, the pixel grayscale is related to the density of the pixels, therefore, high density results in high grayscale value and the low density corresponds to low grayscale value. In this polymer nanoencapsulated templated silica aerogel, it is known that the cell-walls consist of silica coated polymer. Therefore, the consideration about dividing the cell-wall material into two different materials and applying two different materials is possible by assigning the material properties using grayscale information. The diameter of the secondary particles for the X-MP4-T045 is about 1 μm, and the polymer coating weight percentage is about 70% (Leventis *et al.*, 2008). Using above information, the grayscale value to separate silica and polymer coating is 80, in this case silica which has higher density is represented by the pixels with grayscale higher than 80.

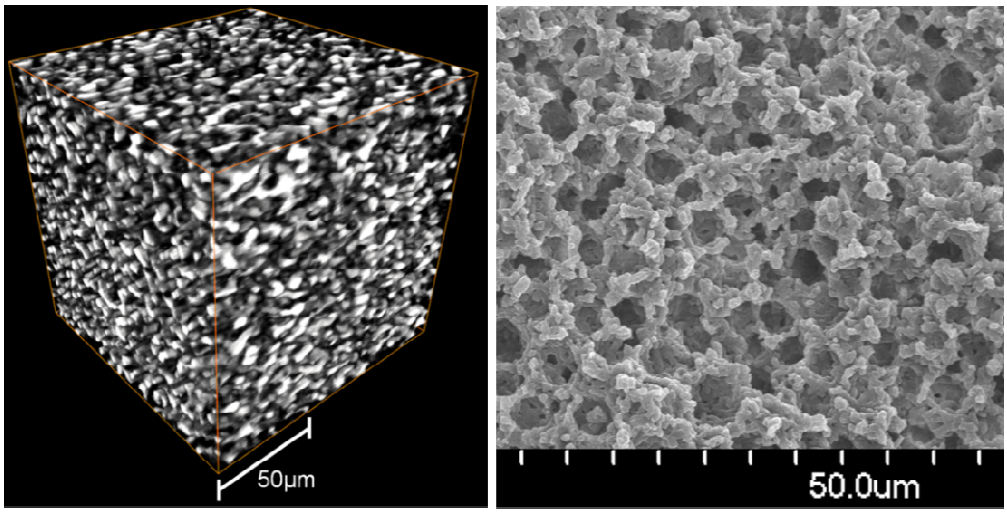

Figure 4.1: (a) nano-CT 3D reconstruction model for X-MP4-T045; (b) Scanning electron micrographs image of X-MP4-T045

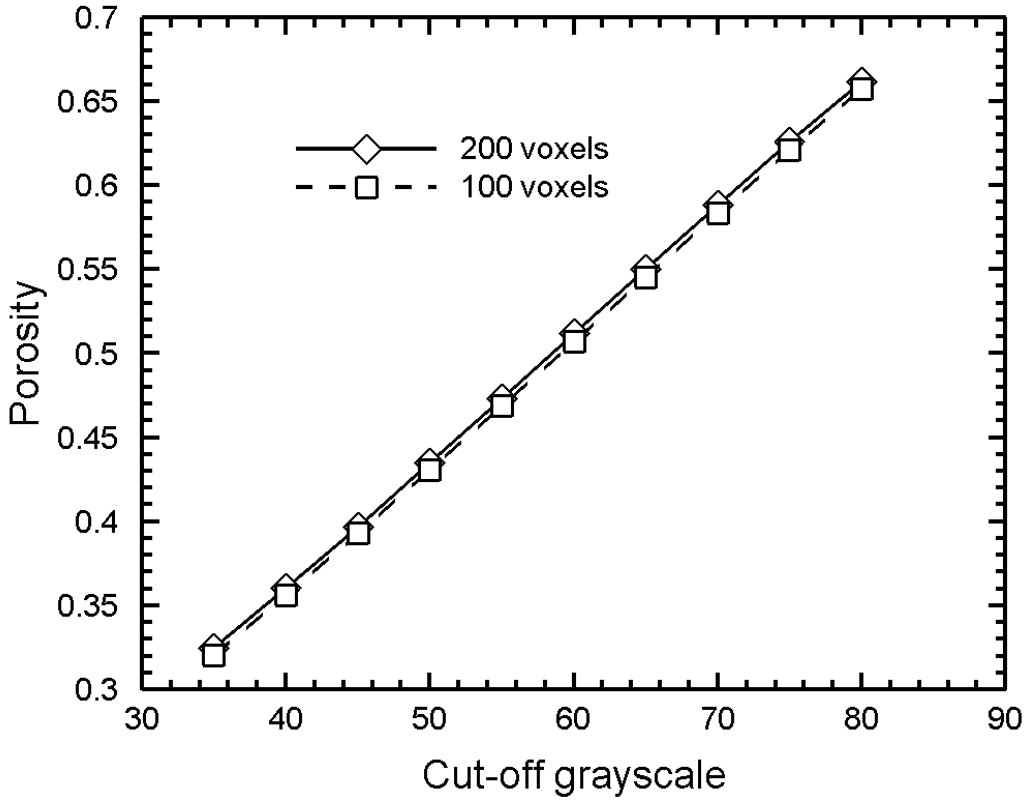

Figure 4.2: Linear relationship between the cut-off grayscale and the porosities from the n-CT image information

4.2 Simulation of X-MP4-T045 under compression at high strain rate

The skeletal density of X-MP4-T045 with bulk density of 0.663 g/cm^3 is 1.320 g/cm^3. The skeletal density of the silica underneath the polymer is 1.935 g/cm^3 (Leventis *et al.*, 2008). In this work, Simulation focuses on the dynamic response; the material properties should have higher values than the corresponding values under quasi-static situation. In this simulation, the Young's modulus of polyurea taken as 6.0 GPa and Poissson's ratio is 0.4; and for the silica, the Young's modulus and Poission's ratio are taken as 70.0 Gpa and 0.17 respectively. The bottom of the aerogel model is fixed loading axial and aerogel lateral surface is traction free. In simulation, when compression is applied through the top plate via velocity loading, a pressure is applied at the top surface immediately. But it takes time for the bottom of the cylinder specimen to feel the stress wave. On the top of the model, a rigid plate, large enough to accommodate expansion of aerogel, was used to apply the velocity boundary condition. The simulation accuracy improves as a finer background grid is used. However, the simulation using the finest background grid (1 voxel for per grid element) is very time-consuming. Consequently, we increased the size of background mesh, eight material points in one cell, in this simulation. The time step used in the simulation is 15.4 ms, which is determined from the longitudinal wave speed of silica-aerogel and gird size. We used following equation to calculate the time step,

$$t_s = \frac{f_c l_c}{C_l},\ 0 < f_c < 1 \qquad (22)$$

where f_c is cell factor, l_c is cell length and C_l is speed of longitudinal wave. In this work, we took f_c =0.1 to allow the wave to propagate across one cell in ten time steps. If the actual velocity used in the SHPB experiment is taken to the model in the simulation, the

simulation time would be very long to reach 70% compressive strain since the small time step used in this dynamic method. To reduce the simulation time, the loading velocity applied was increased to 10 m/s, which results in a strain rate of 1.9×10^{5} s^{-1} in this simulation. In such a dynamic problem the force is initially applied on the top, at that time, the bottom does not feel the wave. The compressive stress wave will travel to the bottom and it will then be reflected back; it usually takes three to five round-trips to allow the force at the top to be nearly equal to the force at the bottom of the sample (Ravichandran *et al.*, 1994). To allow equal forces to apply both top and bottom surfaces of the aerogel, we ramp up the speed at a slow acceleration 2000 m/s^2, after forces are equal on both surfaces we keep the velocity of 10 m/s until simulation is complete. Figure 4.3 (a) shows the simulation output from the top and bottom surface of the model, which indicates the dynamic equilibrium has been reached at around 6% strain.

The size of the silica-aerogel microstructure that can be simulated is limited by the available computational power; therefore we cannot simulate the microstructure deformation on a model size similar to the actual sample used in the SHPB experiments. Alternately, the simulation is carried out for a representative volume element of the silica-aerogel microstructure. From Scanning Electron Micrographs, the average pore size of X-MP4-T045 is about 6~7 μm, and the wall thickness of the microstructure is about 2~3 μm. To determine the appropriate RVE size, we started the simulation using a cube with side length size four times of the pore size (4× pore size), and then we increased the side length incrementally, in this case, up to 8× of the pore size. The results are shown in Figure 4.3. It is seen that as the size increases, the results change. But when the RVE size reaches 6 to 8 times of the pore size, the results are close to each other. In

later simulation, an RVE with side length 8× of the pore size i.e., ≈ 52.8 μm in this case was used as the side length of the cubic RVE. All the RVE models were generated using same cut-off grayscale (58), for each case we also calculated the porosity of different RVE models. The 4× model has the lowest porosity 51%, with model size increasing the porosity decreases and converges to 50%, which is the actual porosity of the silica-aerogel material. Schraad *et al.* (1997) introduced a function of geometric scale parameter, which is defined as the ratio of cell size over representative volume size, to quantify the accuracy of high order term of strain energy. Because the strain energy density converges to its global average as the size of RVE increases, the function should converge to unity when the scale parameter goes to zero. Using this theory, the geometric scale parameter function almost converges to unity when the geometric scale parameter approaches to values about 8 to 9, which agrees with the RVE size decided by running MPM simulations.

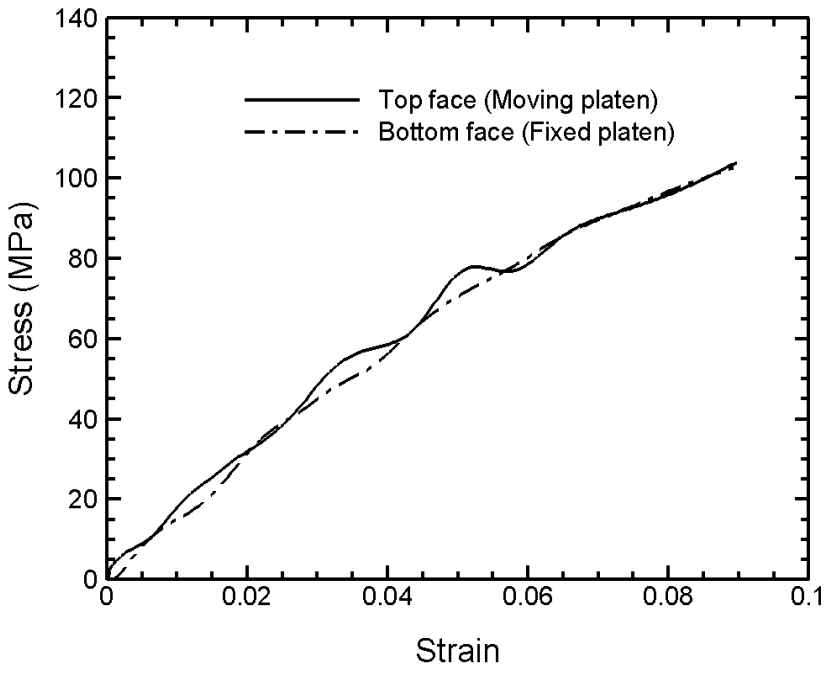

(a)

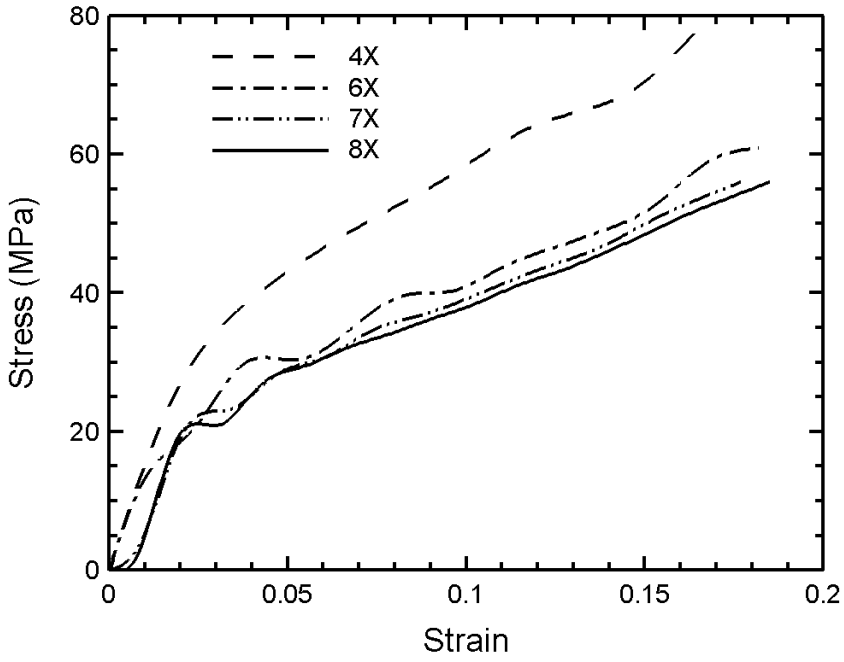

(b)

Figure 4.3: (a) Comparison of stress-strain curves indicating dynamic equilibrium; (b) Comparison of stress-strain curves from different sizes of volume simulations

4.3 Comparison of experimental data and simulation results

4.3.1 Dynamic Compressive SHPB Measurements

Since MPM simulations give high strain rate loading, it is reasonable to compare simulation results with experimental data on the compression of X-MP4-T045 at high strain rates. In this work, the MPM simulation results are compared with the results on the dynamic compressive behavior of a cross-linked templated silica-aerogel using a split Hopkinson pressure bar. This method has been applied to measure compressive behavior of cross-linked silica and vanadia aerogel (with low mechanical impedance) successfully (Luo *et al.*, 2006 & Luo, *et al.*, 2008). The dynamic experimental data from the SHPB

were chosen since the MPM simulation theory is based on the dynamic computation theory. Therefore, the comparison between MPM simulation results and dynamic compressive experimental results is more reasonable than the comparison with static compressive data. The dynamic compressive experiment was carried out modified SHPB equipment developed in our group. A copper disk pulse shaper is used to generate a constant strain rate and reach the dynamic stress equilibrium under SHPB experiments. The schematic diagram of this facility is shown in Figure 4.4.

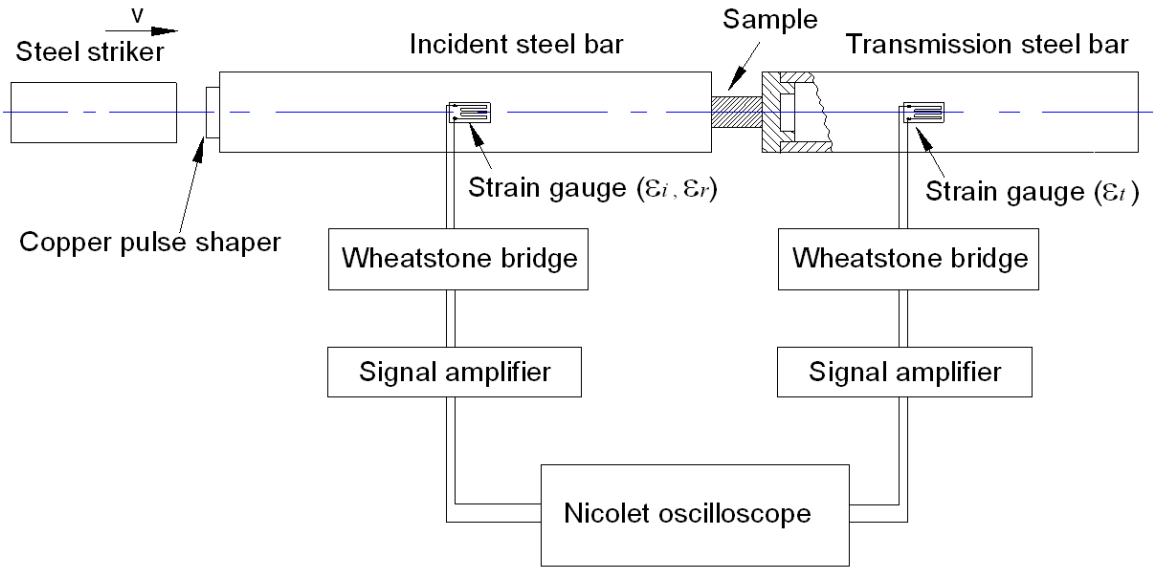

Figure 4.4: Schematic diagram of the SHPB experimental facility, which contains a pneumatic launching system for striker bar, incident and transmission bars, strain acquisition system. A specimen is sandwiched between incident and transmission bars

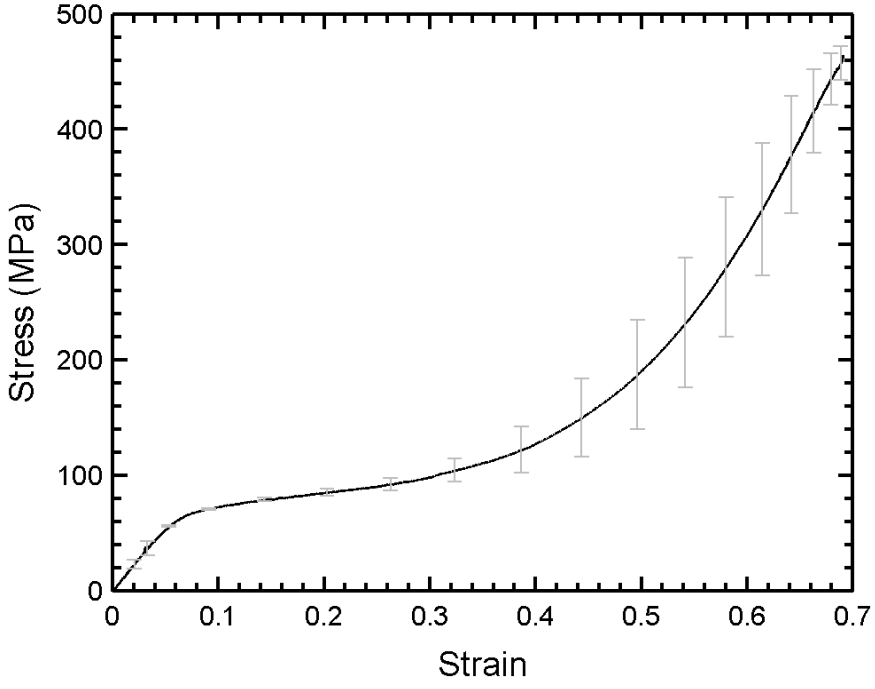

(a)

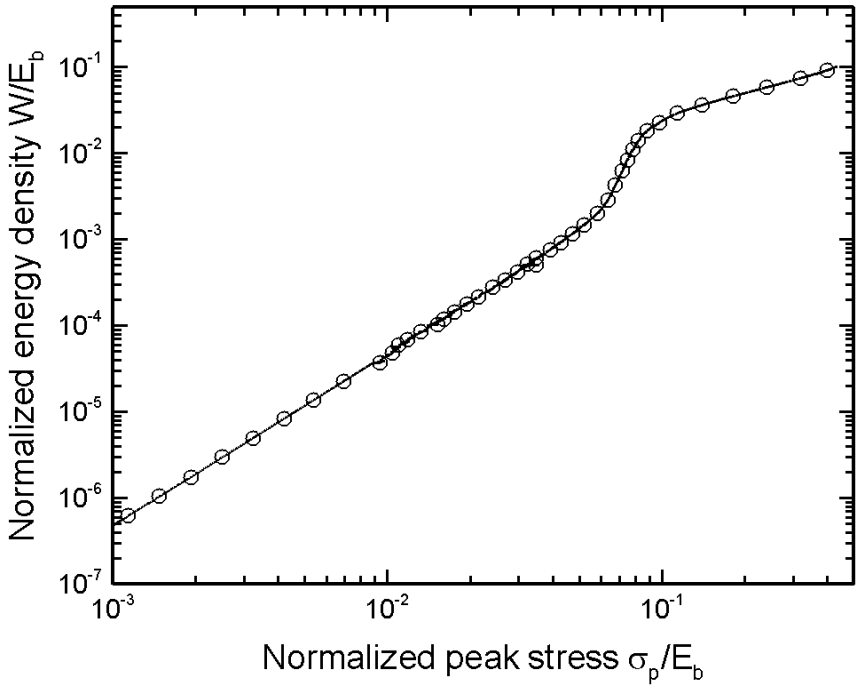

(b)

Figure 4.5: SHPB experimental result of X-MP4-T045: (a) Stress-strain curve at high strain rate (3070 S^{-1}); (b) Energy absorption diagram

All dynamic compressive experiments were conducted under ambient conditions at temperature 20 ± 1 °C and a relative humidity of 22 ± 3%. Cylindrical specimens (10.16 mm in diameter, 2.54 mm thick) were used to measure the stress-strain relationship at high strain rate 3070 s^{-1}. Cross-linked templated silica-aerogel samples with density 0.663 g/cm^3 were used in this SHPB experiment. The stress-strain curve is determined at high strain rate 3070 s^{-1} as shown in the Figure 4.5 (a). In this high strain rate dynamic compressive experiment, the X-MP4-T045 samples are able to deform up to 70% compressive strain. This stress-strain curve shows the typical response of porous materials under compression: a linearly elastic deformation under small strains (< 5%), collapse regime accompanied by plastic hardening until ~ 40% strain, and finally a densification stage. Figure 4.5 (b) shows the normalized energy absorption (W/E_b) as a function of normalized peak stress (σ_p/E_b). In this case, E_b = 1.075 GPa is bulk modulus of silica-aerogel. W is the energy density corresponding to the peak stress, σ_p. The specific energy absorption was calculated as 108 J/g under 70% compressive strain. The lower strain level of densification region is used as densification strain (ε_D = 45%) and is indicated as shoulder area. The specific energy absorption at this strain is 40 J/g.

4.3.2 Simulation of purely elastic properties for the skeleton materials

One of the primary purposes for simulation is to obtain the numerical stress-strain curve using a curve fitting procedure to match with the experimental data by varying the yield stress, hardening coefficient and failure stress of the skeletal material. Initially, a model assigned with purely elastic linear constitutive model in simulation. Figure 4.6 shows the stress-strain relationship for the silica-aerogel model assigned with purely elastic material properties. Unlike the typical feature of a plastic foam response

(Daphalapurkar *et al.*, 2008), the simulation result assigned purely elastic material properties does not show yielding region following an initial elastic region. In this simulation, the initial linear elastic region of the stress-strain curve from MPM simulation agrees well with the experimental data. The densification region follows a longer linear elastic region which is up to almost 30% compressive strain, in which the strain reaches about 46%. The compressive stress along loading direction is about 660 MPa at 46% compressive strain which is much higher than the experimental data already. The stresses carried by some material points are unreasonably high since only elastic properties have been assigned. Figure 4.7 shows the simulation results of initial model (a) and the model at 46% compressive strain in compression (b). The pores in the initial model have been fully compacted when the compressive strain reaches 46% strain. The capability of MPM to deal with large deformation and complex contact problem has been demonstrated apparently in this simulation.

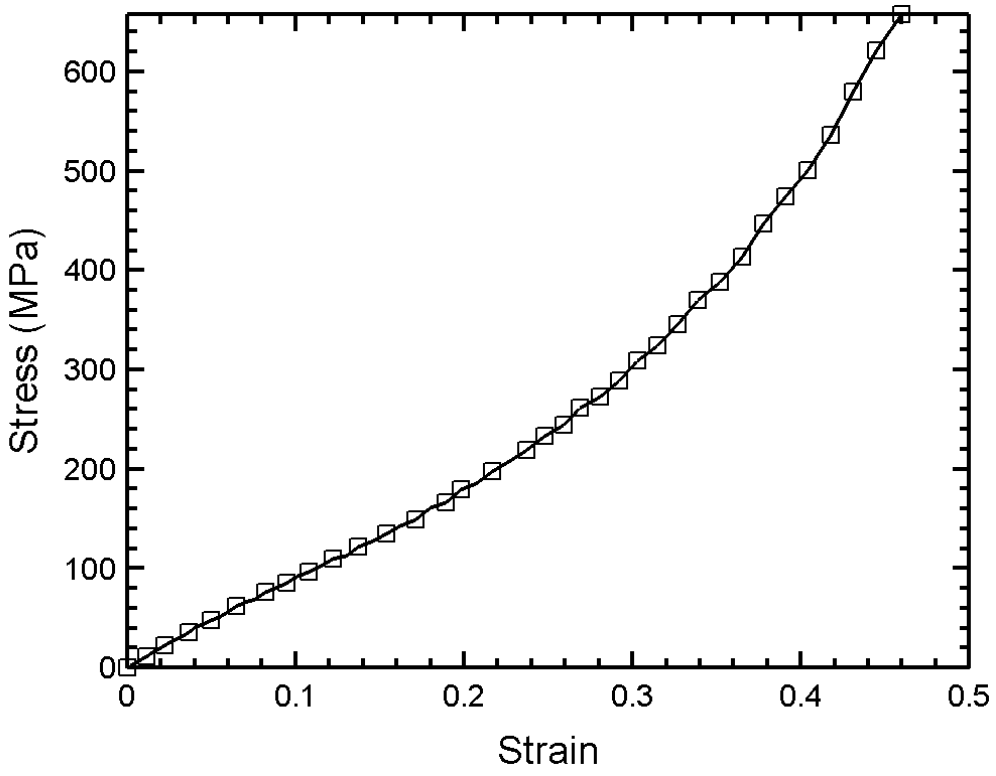

Figure 4.6: Stress-strain curve obtained from MPM simulation using purely elastic properties for the skeleton materials

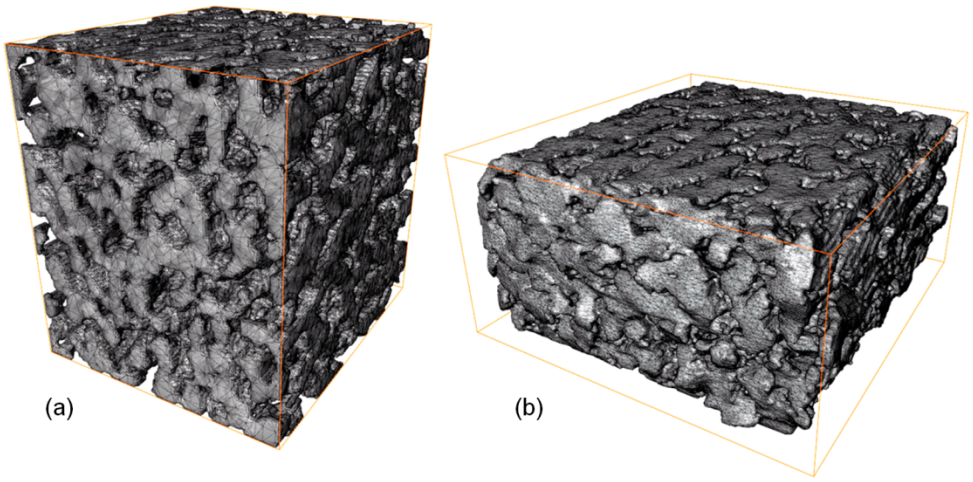

Figure 4.7: Simulation results from the model assigned with purely elastic material properties: (a) The volume rendered image of initial model without loading applied; (b) The volume rendered image of simulation result at 46% strain in compression

4.3.3 Simulation of compaction results

Dynamic testing results from SHPB experiments indicate that cross-linked templated silica-aerogel can absorb energy when subjected to compressive loading. Numerical simulation of the silica-aerogel compaction process handles the large deformations and internal contacts which develop to the closure of the pores during compression. MPM can overcome these two challenging issues as shown in Figure 4.7 because of its inherent capability to deal with internal contacts using the non-slip contact method with the use of the material failure model the points reaching a critical strain (or stress) level are deleted using a failure criterion applied through the MPM code during the simulation of the compaction. Since the material properties come from two different materials, polyurea and silica; one failure criterion used for each material constituent. Silica has low tensile strength but its compressive strength is much higher, therefore the failure of silica contains both tensile failure and compressive failure criteria. A stress failure criterion is applied for materials that fail in tension, and the failure stress is 370 MPa; on the other hand, a strain failure criterion is employed to determine whether the material points will be deleted under compression, and the failure strain used is 150%. Polyurea owns typical polymer material properties, and it can be deformed up to more than 200% strain under either tension or compression even at high strain rates (Roland *et al.*, 2007); in this case, only the strain failure criterion is applied in the simulation. Our simulations can predict the mechanical response of polymer encapsulated surfactant templated silica-aerogels under compression based on the real microstructure obtained using n-CT. To minimize the running time, the simulation was submitted to 16 processors on an OSU cluster. Figure 4.8 shows the stress-strain response of a 50%-porosity cross-

linked templated silica-aerogel model under compression and is compared with the SHPB dynamic experimental results. The curve shows the typical features of a porous material, whereas, the stress increases linearly with strain at small deformations (linear elastic stage), followed by compaction in plastic hardening stage, and a final densification region with the pores squeezed close. In this simulation, the compressive strain can reach up to 70% and the stress-strain curve agrees with the dynamic experimental results extremely well.

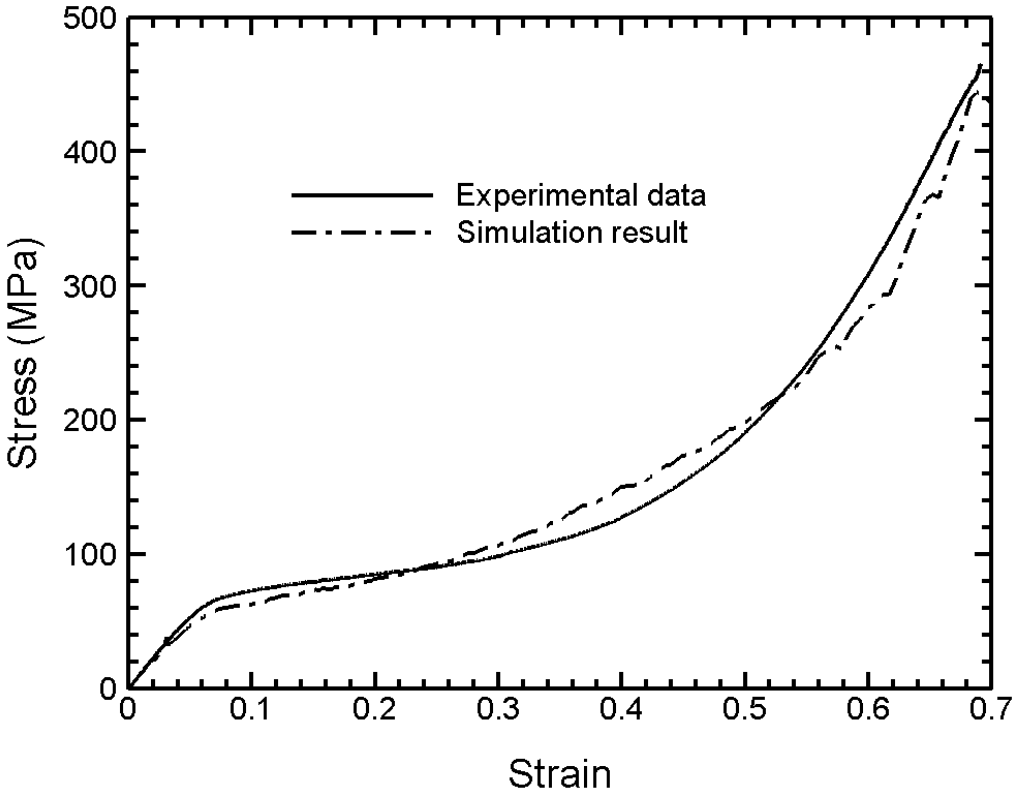

Figure 4.8: Comparison of stress-strain curve obtained from numerical simulation using MPM with experimental results at high strain rate (3070 s^{-1})

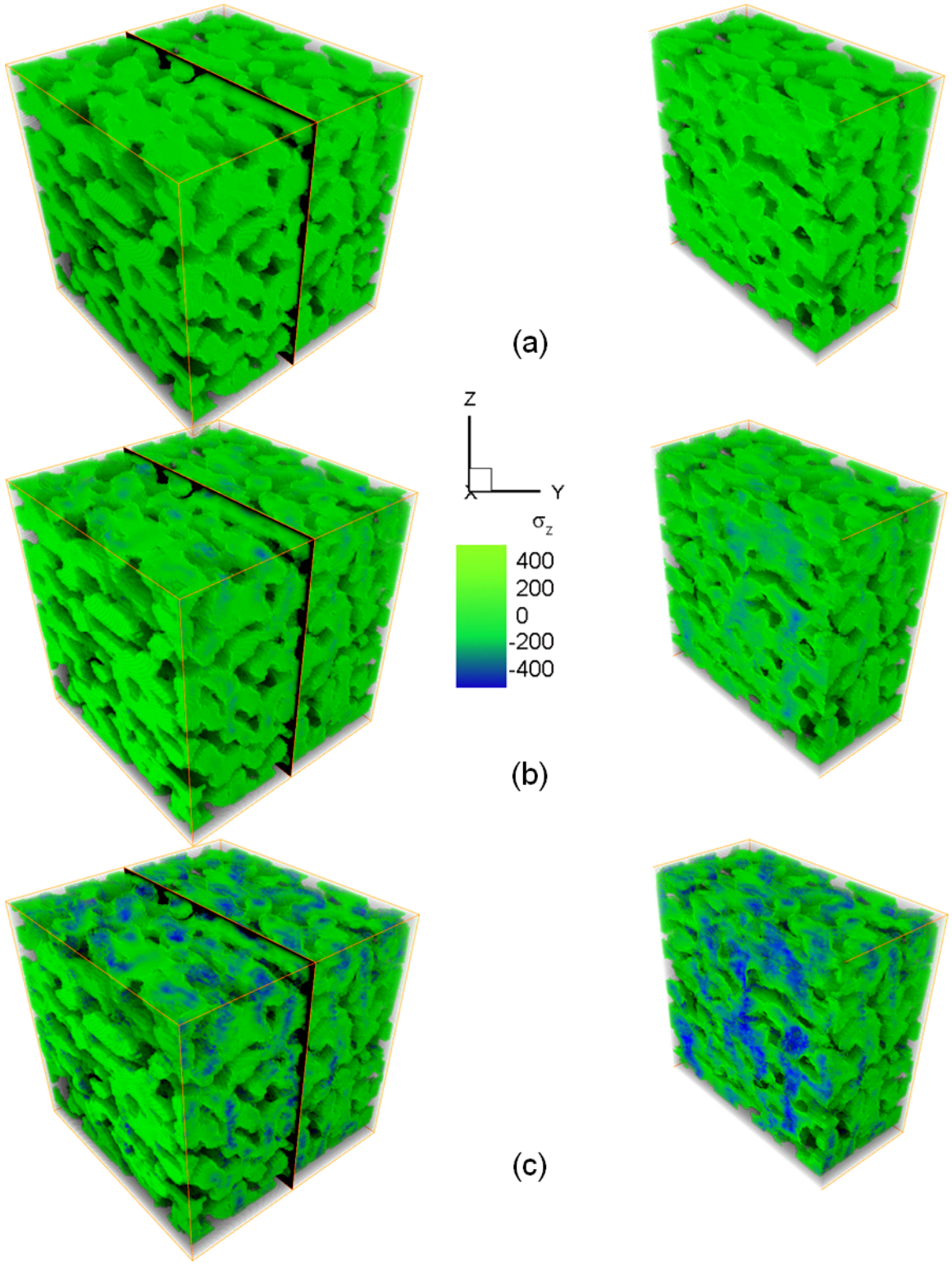
(a)
Z
Y
X
σz
400
200
0
-200
-400
(b)
(c)

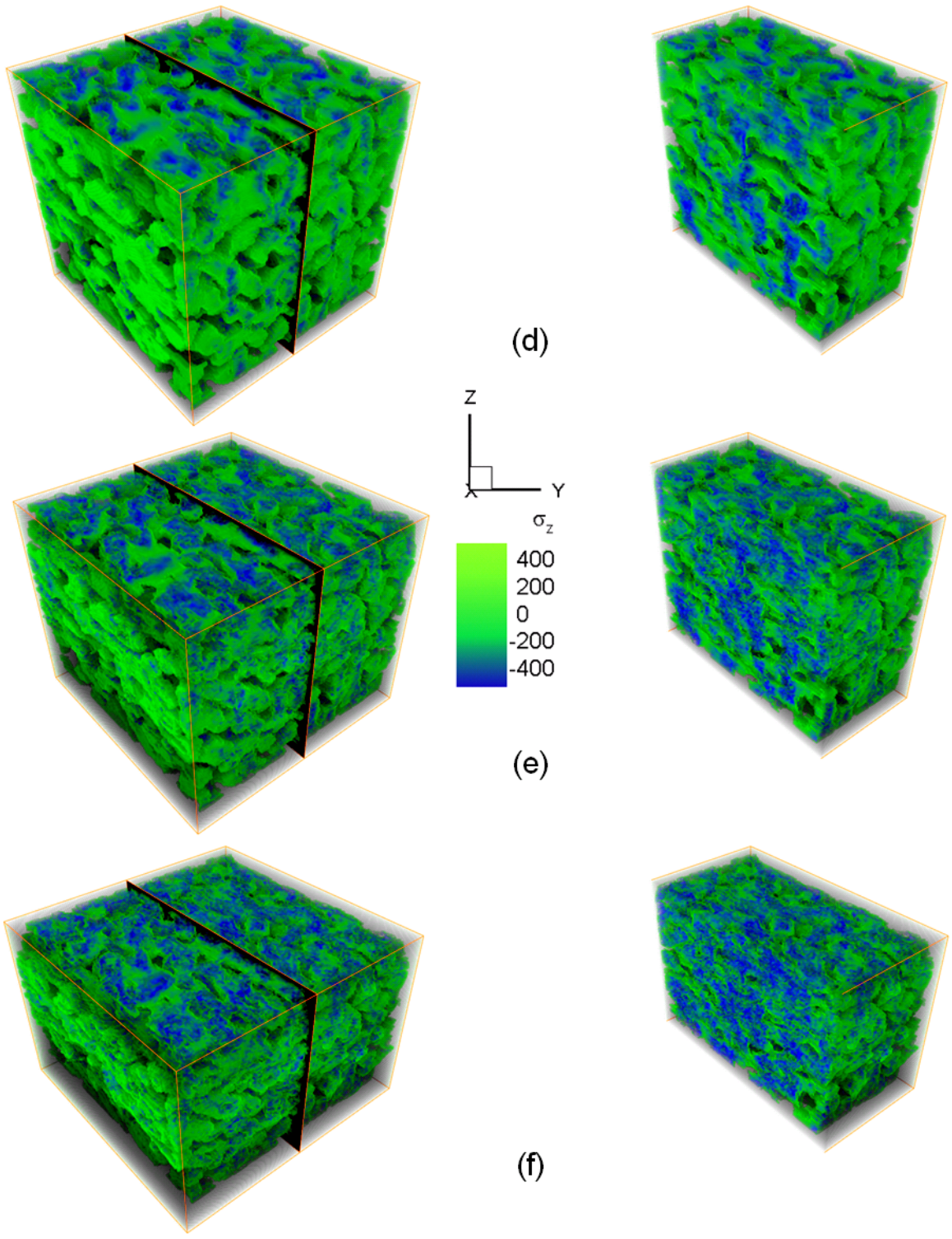
(d)
Z
Y
X
σz
400
200
0
-200
-400
(e)
(f)

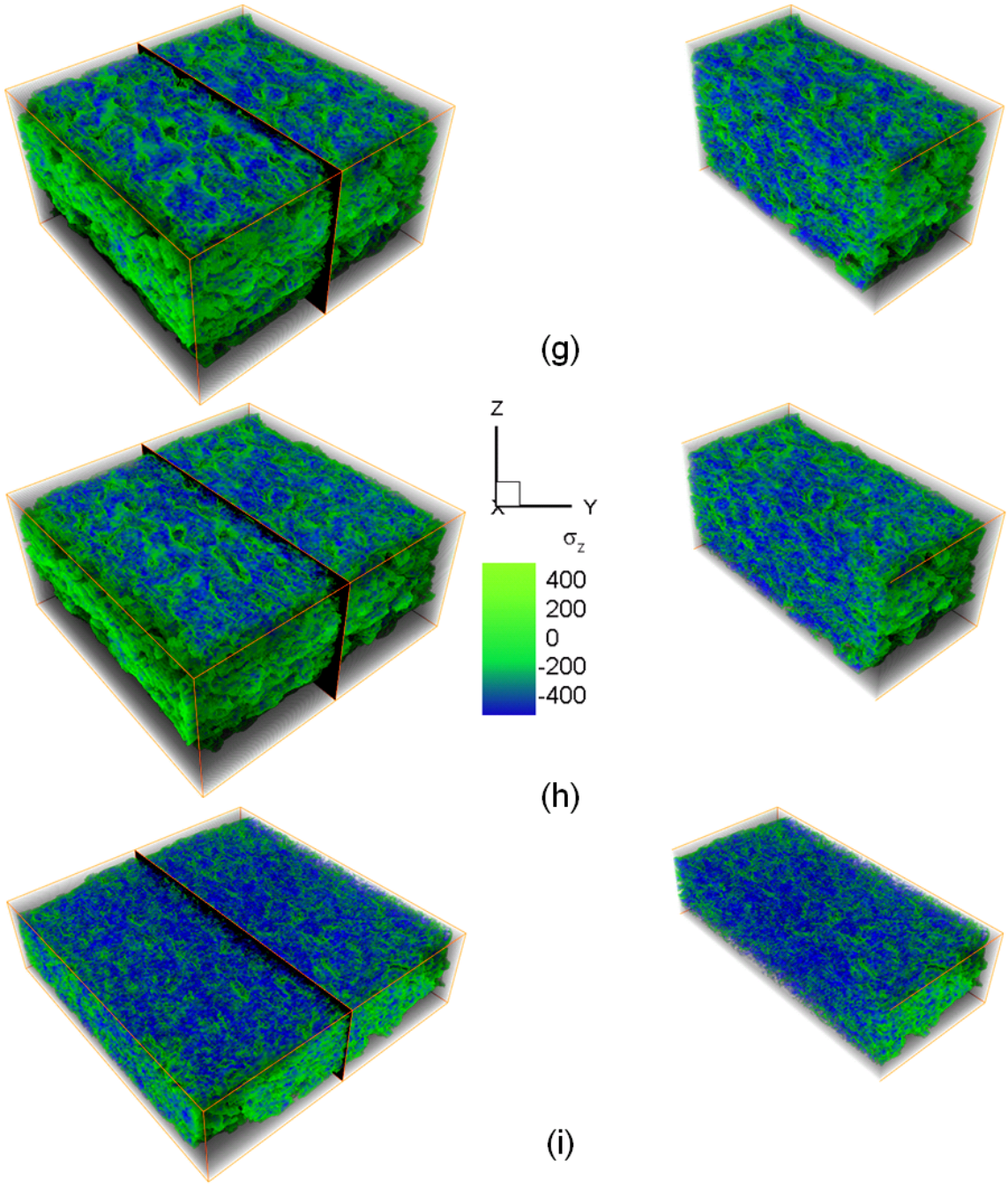

Figure 4.9: Deformed 3D MPM models and sectional views at different compressive strains: (a) Strain = 0; (b) Strain=0.6%; (c) Strain= 5.1%; (d) Strain=6.5%; (e) Strain=18.9%; (f) Strain=30.7%; (g) Strain=39.6%; (h) Strain=49.6%; (i) Strain=70.4%

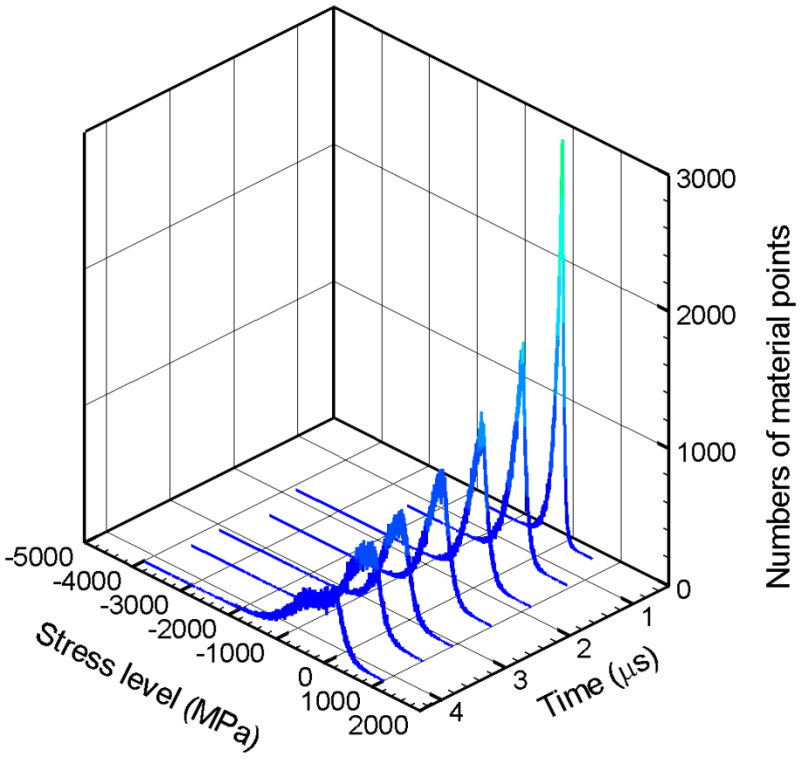
3000
2000
1000
0
Numbers of material points
-5000
-4000
-3000
-2000
-1000
0
1000
2000
Stress level (MPa)
1
2
3
4
Time (μs)

(a)

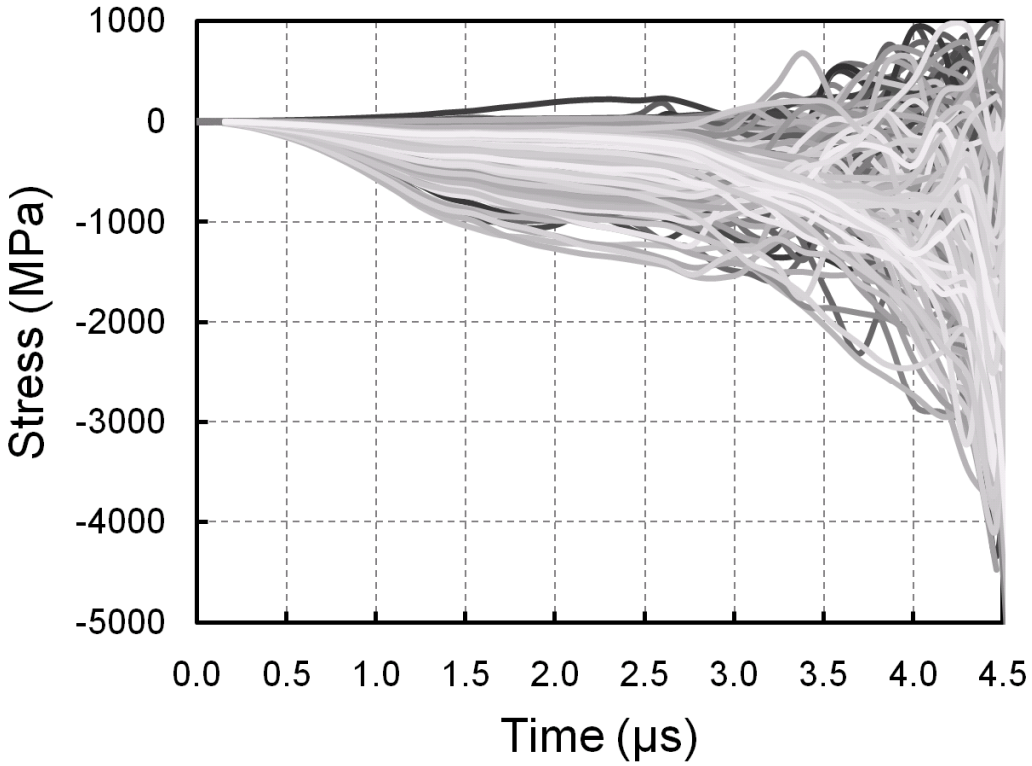
1000
0
-1000
-2000
-3000
-4000
-5000
Stress (MPa)
0.0
0.5
1.0
1.5
2.0
2.5
3.0
3.5
4.0
4.5
Time (μs)

(b)

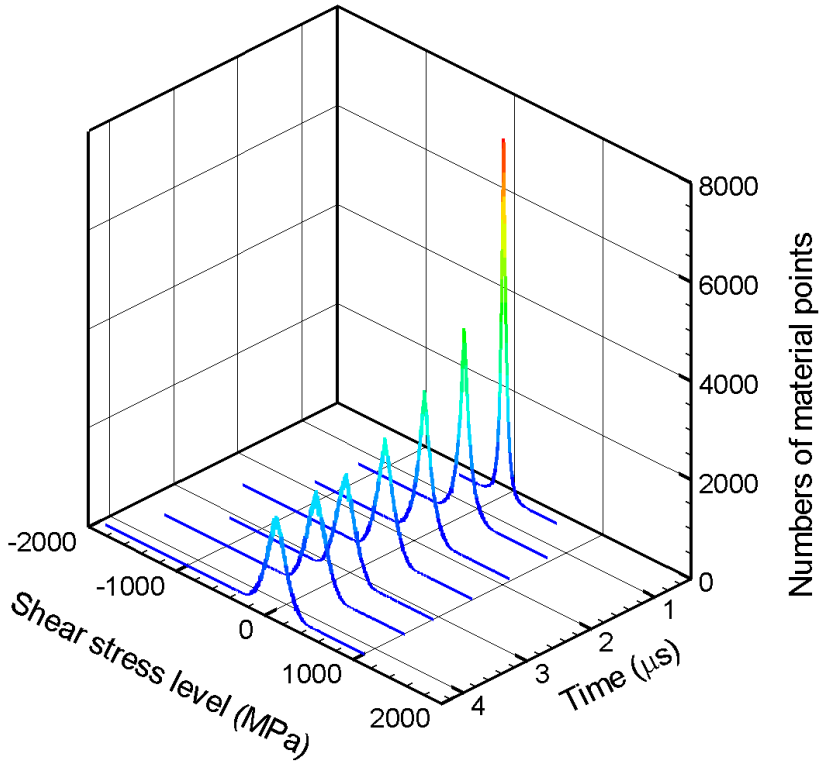

(c)

Figure 4.10: (a) Histogram of the distribution of material points with different stress level at different time; (b) Curves of stress against time from different material points; (c) Histogram of the distribution of material points with different shear stress level at different time

4.4 Discussion

Schradd & Triantafyllidis (1997) explored the macroscopic properties in periodic and nearly periodic microstructures and reported that microstructure imperfection is a critical issue for the periodic and nearly periodic materials response under deformation. This method has been used in foam simulation by Gong *et al.* (2005), showing the effect of imperfection on the stress response. Further work on the crushing simulation of foam (Gong *et al.*, 2006) emphasized the microstructural evolution of the foam structure model. In the work by Gong *et al.* (2005), an imperfection is introduced in the simulation model,

it leads to higher stress levels and a softening response in the field near the imperfection. Because of the propagation of the high stress zone throughout the entire model, a shear band forms between highly deformed zones and less deformed zones. The shear band is oriented at an angle to the macro loading direction, but predicting the magnitude of the angle might be a complicated work (Triantafyllidis *et al*., 1998). Since MPM simulations of silica-aerogels is based on the microstructure determined from n-CT instead of from theoretically generated models with the incorporation of the imperfect structure, the imperfection should already exist in the microstructure of our MPM model. In our previous simulations on closed-cell polymeric foams under compression using the MPM code (Daphalapurkar *et al*., 2008); we reported similar conclusions about the failure along shear band. However, the deformation of polymer cross-linked silica-aerogel is different from typical closed-cell foams with non-uniform deformation characteristics. The strength of cellular material is related to their pore size, which is increasing with the wall thickness and decreasing with pore diameter (Gibson *et al*., 1988). In this work the cross-linked silica aerogels simulated with a smaller pore diameter / wall thickness ratio than typical foam materials, they undergo a uniform structural deformation, which might be caused by the special random but also ordered mesoporous walls (Leventis *et al*., 2008). Figure 4.9 shows the 3D deformation at different nominal compressive strains and the sectional views of the stress distribution along the loading direction from the MPM simulation based on the RVE of cross-linked templated silica-aerogels. The cross-sectional views clearly indicate that the stress chains along the compressive loading direction are distributed nearly uniformly with increase of the nominal strain while the deformed structure does not generate any obvious shear bands causing failure along them.

This behavior is quite different from the compression of plastic foam with high pore diameter / wall thickness ratio in which compaction occurs always at weak planes (shear bands) inducing propagation of compaction waves, which leads to highly localized deformations. Figure 4.10 (a) shows a histogram of the distribution of material points at different stress level and at different time (or strains). The distributions of material points support the stress response shown in Figure 4.9. Within 0 to 1 μs time period (corresponding to 0% to about 6.93% strain), the magnitude of the distribution curve peak decreases rapidly because deformation occurs in the elastic regime; from 1 to 3.5 μs (corresponding to 6.93% to about 62% strain), the magnitude of the distribution curve peak does not change too much, because deformation occurs in the non-elastic plateau region where the microstructure collapses; and finally the peak of the distribution curve at 4 μs (about 74% strain) has been greatly decreased because of densification. In Figure 4.10 (b), the curves of stress as a function of time from different material points are plotted. Because the simulation concerns compression, there are more curves in the negative side at the beginning of the simulation. In this plot, the stress curves stay in a narrow range in the elastic and plateau region (from 0 to 3 μs), but much higher stresses appear when the deformation enters the densification region where the material is mostly compressed.

It is known that the propagation of a local buckling in the microstructure results in the evolution of microstructure collapse, and the instability of buckling causes the energy stored in the stress field to be exhausted by localized shearing, which in turn contributes to the formation of the shear band (Demetriou *et al*., 2007). Since the uniform deformation observed here occurs in a random microstructure of a polymer cross-linked

surfactant template silica-aerogel, the stress concentration is averaged out throughout the entire structure thus reducing the stress difference between the highly deformed zones and the less deformed ones. The shear band angle is still under development, and the shear stress information is more important. The uniform deformation without apparent shear banding zone has been described above, in this case, the shear stress results should be able to support this conclusion too. Figure 4.10 (c) shows the histogram of the distribution of material points with different shear stress level at different time (strain) respectively. From the histograms at different time, we can find the shear stress distribution is even more uniform than the stress along loading direction, which can support the fact that the uniform deformation without shear band very well.

4.5 Effects of porosity as determined from simulations

Since polymer coating cross-linked improves the mechanical properties of the underlying silica-aerogel dramatically, it is critical for the design and improvement of cross-linked aerogels, to simulate the function of the polymer coating using MPM. For this purpose, we considered three different types of silica-aerogel models, which all can be prepared readily through current techniques (Leventis *et al.*, 2007 & 2008). Figure 4.11 shows a cross-sectional view of the stress distribution at two strains level (19% and 30%) for models with different porosities are. For this, three simulations have been run: (a) 70% porosity MPM model assigned only silica material properties; (b) 70% porosity MPM model assigned polymer and silica material properties; (c) 50% porosity MPM model assigned polymer and silica material properties. The porosities in the model have been controlled using the grayscale as discussed previously in this paper. Since the typical foam porosities are about or more than 70%, our simulations are run on models

with 70% porosity for comparison of the microstructural evolution. Because the polymer coating plays an important role in the material properties of cross-linked silica-aerogel, models with and without polymer coating were examined. The volume ratio of the polymer and the silica is same in both of 70% porosity and 50% porosity models assigned with same polymer and silica material properties. The same loading conditions and failure criteria which were introduced previously for polymer and silica were employed in all these new simulations.

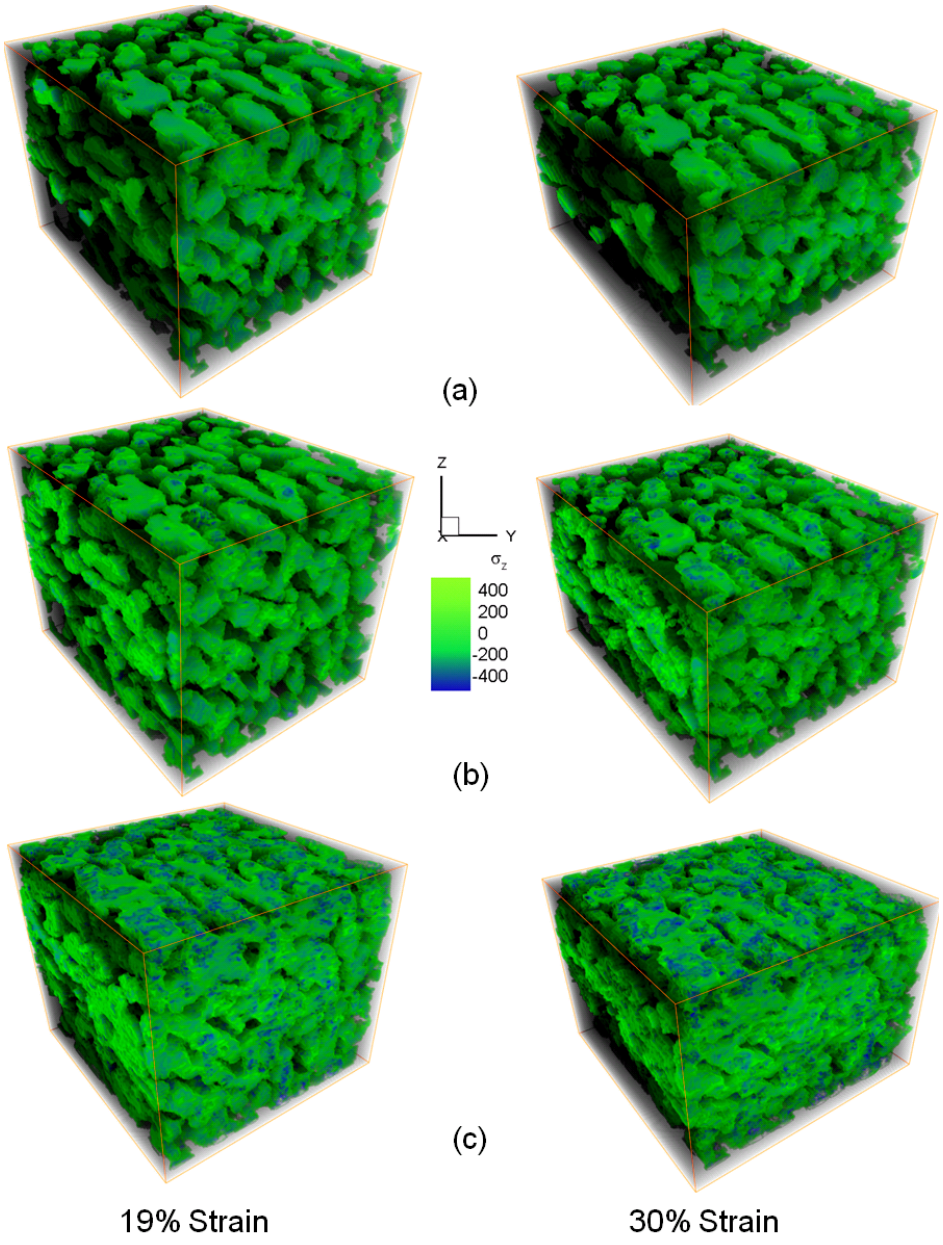

Figure 4.11: 3D view of stress distribution at different compressive strains from models with different porosities: (a) 70% porosity model assigned only silica material properties; (b) 70% porosity model assigned polymer and silica material properties; (c) 50% porosity model assigned polymer and silica material properties

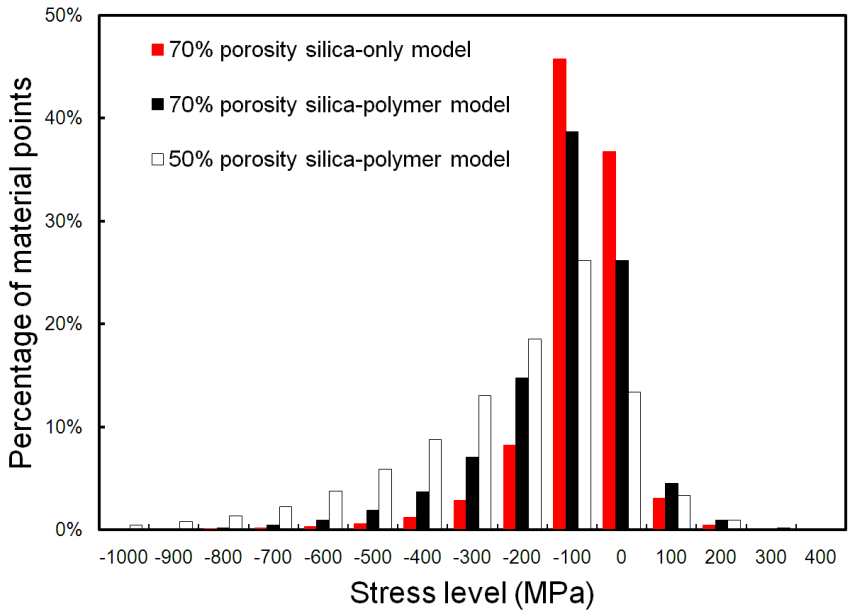

(a)

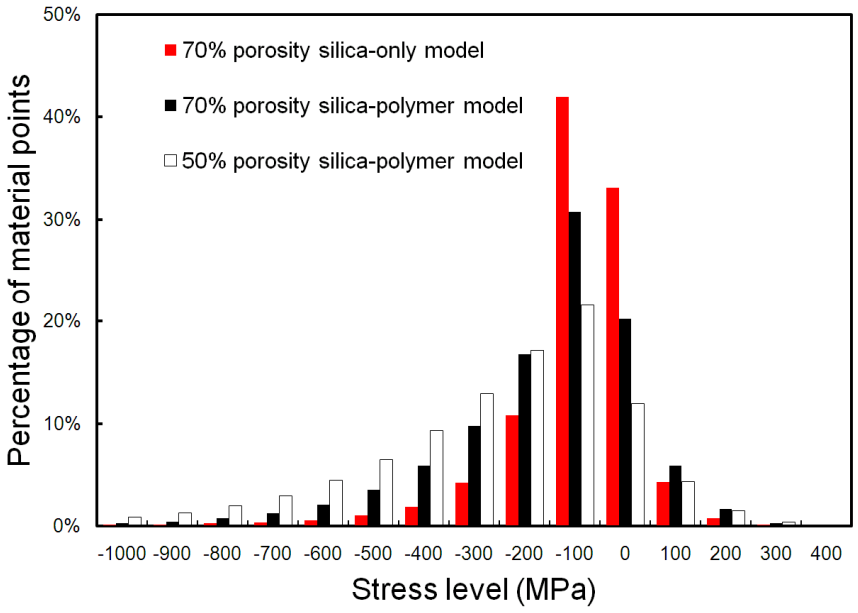

(b)

Figure 4.12: Histograms of the distribution of percentage of material points with different stress levels at different strains: (a) Data from 19% strain deformation; (b) Data from 30% strain deformation

In Figure 4.11, stress chains along loading direction in 70% porosity model assigned only silica material properties are not as clear as which shown in models assigned polymer and silica material properties in the same figure. Meanwhile, the skeleton wall for silica only model has already failed at 30% strain level since silica with lower strain failure criterion and cannot be applied high load in this structure. On the other hand, the 70% porosity model assigned both of polymer and silica material properties does not show obviously material failed and stress chains are also generated along the loading direction which mean this structure with polymer coating has capability to carry much higher load. The bottom two pictures in Figure 4.11 show that the stress chains dominate the entire area in either 19% or 30% compressive strain level and 50% porosity model with two material properties assigned gives the most uniform stress distribution. Figure 4.12 indicates a histogram of distribution of material points (in percentage) with stress level at two different strains (19% and 30%). Stresses distribute in a wider range in the histograms of 50% porosity model from Figure 4.12, which means that more material points start to carry load in this case and the stress gradient of stress distribution is lower than 70% porosity models. Although the 70% porosity model with two material properties has higher stress that of the gradient, it is still much lower than the one with silica only even the porosities are identical. The models assigned with two material properties have lower stress distribution gradient and they should have less chance to induce local stress concentration than the model with only one material property assigned, consequently they can absorb more energy and fail only at high strain level.

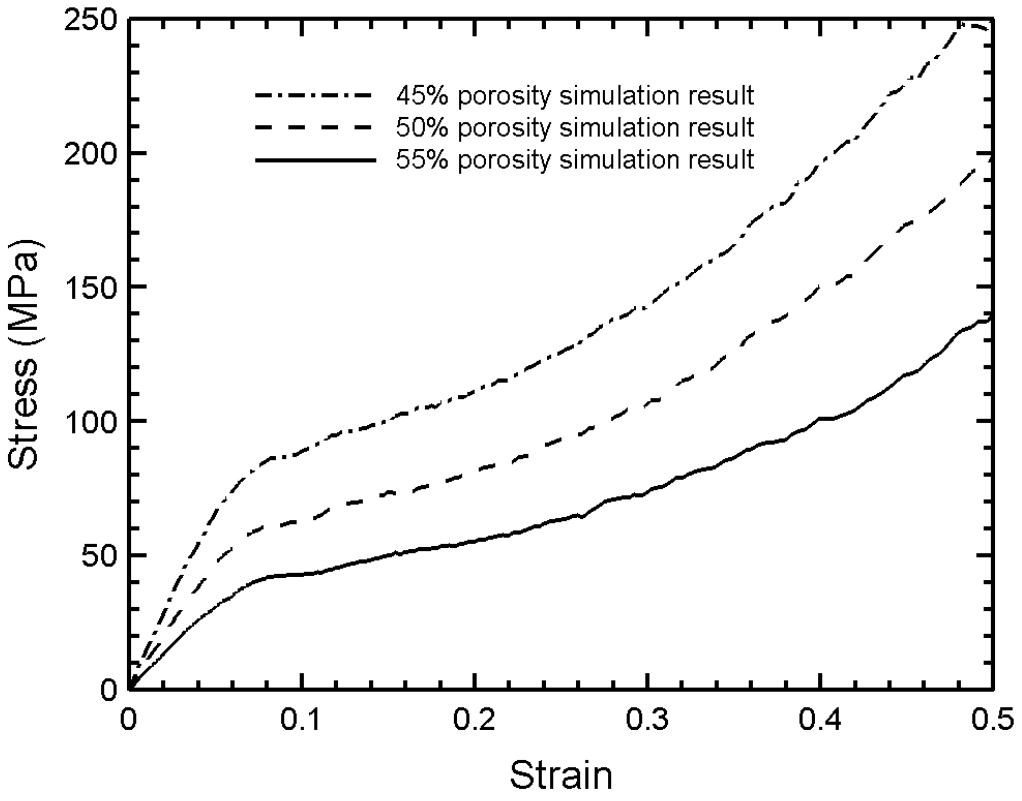

Figure 4.13: Compressive stress-strain curve for model with different porosities obtained from numerical simulation using MPM

As described in the previous part of this work, we are also interested in the network morphology of cross-linked aerogel too. As the first step of work along this direction, the models with different porosities are used in simulations. The relation between global density (porosity) of silica-aerogel and mechanical properties has been investigated through experimental measurement (Woignier *et al.*, 1987 & 1989). In this work, we would like to use numerical method to explore this phenomenon. The previous work shows the relationship between the bulk density and mechanical properties. Increasing bulk density would reduce the porosity of materials. In this case, the relationship between density and mechanical properties can also be described as a

relationship between porosity and mechanical properties. Figure 4.13 shows the stress-strain curves for models with three different porosity values, namely, 45%, 50% and 55%. In these simulations, the change of porosity is controlled by increasing the thickness of polymer coating layer, in the mean time there is no change for the amount of silica. Since the procedure described in this assumption can also be implemented by using cross-linking technique as well, the simulation results can potentially be used to improve mechanical properties of aerogels.

The response of silica-aerogels with different densities (porosities) under compression can be explained by considering an analog model of silica-aerogel. It is reasonable to assume that the highly porous silica-aerogel network is composed of hinge- and beamlike structures. According to the statistical growth procedure of the aerogel these beams are usually bent like "knees" instead of straight form (Gross *et al*, 1992). When the silica-aerogel is applied with compressive load, the knee angles are reduced which causes the beam structure weaker. Furthermore, the stiffness of beam structure decreases as the length increases and section area decreases, in this case the beams can be bent in an easier manner. This fact shows the density dependence of modulus: increasing bulk density will lead to the bigger sectional area and relative shorter beam length, which will reduce the bending effect. Several previous works (Woignier *et al.*, 1987 & 1989) on the measurement of the mechanical properties of silica-aerogels have been conducted, and a power law relationship has been found between the Young's Modulus and the aerogel densities ρ (porosities):

$$E \sim \rho^{\alpha} \tag{23}$$

where α ≈ 3.8. Gibson & Ashby (Gibson *et al*., 1988) developed a theory which describes the behavior of cellular solids based on the assumption that the structure of the cells behaves like beams. The method is widely used to analyze the mechanical response of the materials with honeycomb microstructure similar to foam. In this method, the hexagonal structure is assumed to be the microstructure of the foam. However, this method is developed based on a monodisperse distribution of pore size model (honeycomb structure), which is not an ideal way to model the materials like aerogel with a large range of pore size and random pore distribution (Pirard, 1997). Scherer *et al.* (1995) has established a relationship between exponent α and the microstructure of aerogel. Instead of assuming a beam structure model, they evaluated their method by using the relationship between bulk modulus, *K*, and the volume dilatation at different stages of the sample:

$$dP = -K\frac{dV}{V}, \tag{24}$$

where *P* is pressure and *V* is the volume. When strains are small, the equation (24) is the definition of elastic bulk modulus, which is constant. In the plastic deformation regime, Scherer *et al.* defined a power law function between bulk modulus and the volume:

$$K(V) = K_0(\frac{V_0}{V})^m. \tag{25}$$

Under small strains, they determined the elastic modulus follows a power law relationship with density with an exponent of 3.6; in the plastic regime, the modulus and density obey a power law relationship as well, but the exponent is ~ 3.2.

By using these power law relationships, we used the certain porosity simulation (based on 55% porosity model) to predict the behavior of cross-linked aerogels with different porosities and the prediction is shown in the Figure 4.14. In the figure, the

prediction results match with the simulation results very well before the curve reaches 30% compressive strain, after that the structure is deformed already and the power law relationship will not be reliable in this stage. Consequently, the power law relationship between the modulus and different densities (porosities) can be predicted by the MPM simulation of silica-aerogel under compression very well. The simulation results are able to capture the material behavior in densification period, in which the power law relationship. The prediction gives lower accuracy at larger deformation in that bending effect becomes less significant for higher densities and thus the response of silica-aerogel model is determined by material properties themselves instead of by the beamlike structural response.

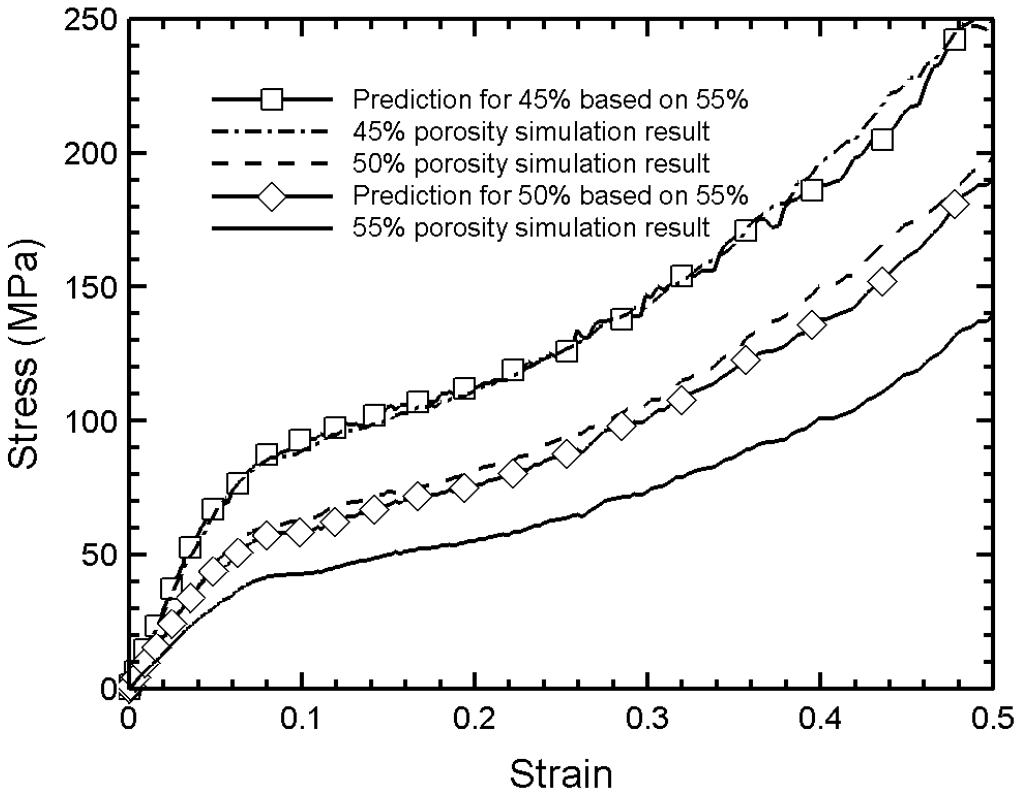

Figure 4.14: Prediction results based on the simulation results following the power function relationship

CHAPTER V

CONCLUSION

In this investigation, the MPM method has been used to simulate the compression of the cross-linked templated silica-aerogel (X-MP4-T045) using the microstructure model reconstructed from n-CT scanning images. Reconstruction of MPM model could be done by controlling the cut-off grayscale of n-CT images, and a linear relation of porosity and grayscale has been reported in this work. As known that the cell-walls of cross-linked templated silica-aerogel consist of silica secondary particles and polymer coating on them, due to their material properties different with each other, it is more reasonable to assign different material properties to these two materials. To solve this problem, the relation between grayscale and density, which is higher grayscale represents higher density, has been employed to separate two different materials. In the simulation, it is proved that the MPM method can handle the large deformation (even up to 70%) and complex internal structure contacts within the densification region. MPM method was developed based on the dynamic method; therefore the simulation results are compared with the experimental results from dynamic SHPB tests. The simulation result obtained from MPM simulation based on the model assigned with elastic only material properties shows good agreement in the linear elastic region. The stress-strain curve obtained from model considered plastic and failure properties matches with the dynamic experimental

results very well in three typical stages of porous material under compression. The stress chains along the loading direction indicate the microstructure deformation evolution is uniform during three deformation stages without obvious shear bonding zone occurs.

Based on the previous work on design space of aerogel, we run several simulations on models with different characteristics. The investigation of these simulations indicates that the stress distribution and the microstructure evolution are affected by both of the polymer coating and the porosity. As the first step of this purpose, different simulations have been run on the model with different porosities and material properties to explore the effects of porosity and polymer coating. The simulation results show the histograms for 50% porosity model assigned two material properties of stress distribution along loading direction, showing stresses distribute in a relatively wider range at same compressive strain level, indicating that more material points start to carry load and the whole microstructure has a lower stress distribution gradient. In this case, the microstructure has less chance to generate stress concentration locally and is able to stand to high compressive strain level. Even with same porosity, the model assigned silica and polymer material properties has lower stress distribution gradient than the one with silica only property assigned, which prove the important role polymer coating plays for cross-linked silica-aerogel again. The effect of porosity was simulated for three different values of the porosity (45%, 50%, 55%) in this work. Results show that the stress-strain relation follows the power law relation obtained from previous work with mass density for porosity ranging from 45% to 55%. The simulation also indicates the power law relation is not suitable when the compressive strain is higher than 30%, due to that the bending effect becomes insignificant for larger densities (most of microstructure

has been compacted in this stage) and thus the response of silica-aerogel model are determined by inherent material properties more instead of beamlike structure. The results in this work show the capabilities of using MPM to simulate the mechanical response and microstructure property relationship of cross-linked templated silica-aerogel, and can be used as the first-step information to improve the design of cross-linked aerogel.

REFERENCES

Bardenhagen, S., Brydon, A., Guilkey, J., 2005. Insight into the physics of foam densification via numerical simulation. Journal of the Mechanics and Physics of Solids 53 597-617.

Bardenhagen, S., Guilkey, J., Roessig, K., Brackbill, J., Witzel, W., Foster, J., 2001. An improved contact algorithm for the material point method and application to stress propagation in granular material. Computer Modeling in Engineering & Sciences 2 (4) 509-522.

Bardenhagen, S. and Kober, E., 2004. The generalized interpolation material point method. Computer Modeling in Engineering & Sciences 5 (6) 477-496.

Brackbill, J., Ruppel, H., 1986. FLIP: a method for adaptively zoned, particle-in-cell calculations of fluid flows in two dimensions. Journal of Computational Physics 65 314-343.

Brackbill, J., Kothe, D., Ruppel, H., 1988. FLIP: a low-dissipation, particle-in-cell method for fluid flow. Computer Physics Communications 48 25-38.

Daphalapurkar, N., Hanan, J. Phelps, N., Bale, H., Lu, H., 2008. Tomography and simulation of microstructure evolution of closed-cell polymer foam in compression. Mechanics of Advanced Materials & Structures 15 594-611.

Demetriou, M., Hanan, J., Veazey, C., Di Michiel, M., Lenoir N., 2007. Yielding of metallic glass foam by percolation of an elastic buckling instability. Advanced

materials 19 1957-1962.

Fricke, J., 1992. Aerogels and their applications. Journal of Non-Crystalline Solids 147&148 356-362.

Gibson, L., Ashby, M., 1997. Cellular Solids: Structure and Properties, 2nd Edition, Cambridge University Press.

Gong, L., Kyriakids, S., Triantafyllidis, N., 2005. On the stability of Kelvin cell foams under compressive loads. Journal of the Mechanics and Physics of Solids 53 771-794.

Gong, L., Kyriakides, S., 2006. On the crushing stress of open cell foams. Journal of Applied Mechanics 73 807-814.

Good B., 2006. Computer simulation of fracture in aerogels. In: Material Research Society Symposium Proceeding.

Harlow, F., 1964. The particle-in-cell computing method for fluid dynamics. Methods for Computational Physics 3 319-343.

Hornung, R., Kohn, S., 2002. Managing application complexity in the SAMRAI object-oriented framework. Concurrency and Computation: Practice and Experience 14 347-368.

Jones, S., 2006. Aerogel: Space exploration applications. Journal of Sol-Gel Science and Technology 40 351-357.

Leventis, N., Sotiriou-Leventis, C., Zhang, G., Rawashdeh, A., 2002. Nanoengineering strong silica aerogels. Nano letters 2(9) 957-960.

Leventis, N., 2007. Three-dimensional core-shell superstuctures: mechanically strong aerogels. Accounts of Chemical Research 40 874-884.

Leventis, N. Mulik, S., Wang, X., Dass, A., Patil, V., Sotiriou-Leventis, C., Lu, H., Churu, G., Capecelatro, A., 2008. Polymer nano-encapsulation of template mesoporous silica monoliths with improved mechanical properties. Journal of Non-crystalline Solids 354 632-644.

Leventis,N., Mulik, S., Wang, X., Dass, A., Sotiriou-Leventis, C., Lu, H., 2007. Stresses at the interface of micro with nano. Journal of the American Chemical Society 129 10660-10661.

Luo, H., Lu, H., Leventis, N., 2006. The compressive behavior of isocyanate-crosslinked silica aerogel at high strain rates. Mechanics Time-Dependent Materials 10 83-111.

Luo, H., Churu, G., Fabrizio, E., Schnobrich, J., Hobbs, A., Dass, A., Mulik, S., Zhang, Y., Grady, B., Capecelatro, A., Sotiriou-Leventis, C., Lu, H., Leventis, N., 2008. Synthesis and Characterization of the Physical. Chemical and Mechanical Properties of Isocyanate-Crosslinked Vanadia Aerogels. Journal of Sol-Gel Science and Technology 48 113-134.

Ma, J., Lu, H., Wang, B., Roy, S., Hornung, R., Wissink, A., Komanduri, R., 2005. Multiscale simulations using generalized interpolation material point (GIMP) method and SAMRAI parallel processing. Computer Modeling in Engineering & Sciences 8 (2) 135-152.

Ma, J., Lu, H., Komanduri, R., 2006. Structured mesh refinement in generalized interpolation material point (GIMP) method for simulation of dynamic problems. Computer Modeling in Engineering & Sciences 12 (3) 213-227.

Ma, J., Lu, H., Wang, B., Roy, S., Hornung, R., Wissink, A., Komanduri, R., 2005. Multiscale simulations using generalized interpolation material point (GIMP) method and molecular dynamics (MD). Computer Modeling in Engineering & Sciences 14 (2) 101-118.

Moner-Girona, M., Martinez, E., Roig, A., Esteve, J., Milins, E., 2001. Mechanical properties of silica aerogels measured by microindentation: influence of sol-gel processing parameters and carbon addition. Journal of Non-Crystalline Solids 285 244-250.

Nakanishi, K., 1997. Pore structure control of silica gels based on phase separation. Journal of Porous Materials 4 (2) 67-112.

Pierre, A. C., Pajonk, G., 2002. Chemisty of aerogels and their application. Chemical Reviews 102 4243- 4265.

Pirard, R., Priard, J., 1997. Aerogel compression theoretical analysis. Journal of Non-crystalline solids 212 262-267.

Primera, J., Woignier T., Hasmy A., 2005. Pore structure simulation of gels with a binary monomer size distribution. Journal of Sol-Gel Science and Technology 34 (3) 273-280.

Ravichandran, G., Subhash, G**.,** 1994**.** Critical-Appraisal Of Limiting Strain Rates For Compression Testing Of Ceramics In A Split Hopkinson Pressure Bar**.** Journal of the American Ceramic Society 77 (1) 263-267.

Roland, C., Twigg, J., Vu, Y., Mott, P., 2007. High strain rate mechanical behavior of polyurea. Polymer 48 574-578.

Scherer, G., Smith, D., Qiu X., Anderson, J., 1995. Compression of aerogels. Journal of Non- Crystalline Solids 186 316-320.

Schraad, M., Triantafyllidis, N., 1997. Scale effects in media with periodic and nearly periodic microstructures, Part 1; Macroscopic properties. Journal of applied mechanics 64 751-762.

Sulsky, D. Zhou, S., Schreyer, H., 1995. Application of a particle-in-cell method to solid mechanics. Computer Physics Communications 87 236-252.

Tan, H., Nairn, J., 2002. Hierarchical, adaptive, material point method for dynamic energy release rate calculations. Computer Methods in Applied Mechanics and Engineering 191 2095-2109.

Triantafyllidis, N., Schraad, M., 1998. Onset of failure in aluminum honeycombs under general in-plane loading. Journal of the Mechanics and Physics of Solids 46 (6) 1089-1124.

Wang, B., Karuppiah, V., Lu, H., Roy, S., Komanduri, R., 2005. Two-dimensional mixed mode crack simulation using the material point method. Mechanics of Advanced Materials and Structure 12 471-484.

Woigner,T., Phalippou, J., 1989. Scaling law variation of the mechanical properties of silica aerogels. Revue De Physique Appliquee C4-179-184.

Woignier, T., Pelous, J., Phalippou, J., Vacher, R., Courtens, E., 1987. Elastic properties of silica aerogels. Journal of Non-Crystalline Solids 95&96 1197-1202.

VITA

Boshen Fu

Candidate for the Degree of

Master of Science

Thesis: SIMULATION OF MICROSTRUCTURAL EVOLUTION OF CROSS-LINKED TEMPLATED SILICA-AEROGELS UNDER COMPRESSION

Major Field: Mechanical Engineering

Biographical:

Personal Data:

Education:
Completed the requirements for the Master of Science or Arts in your major at Oklahoma State University, Stillwater, Oklahoma in December, 2009. Received Bachelor of Engineering degree in Mechanical Design Manufacture & Automation from East China University of Science & Technology, Shanghai, China in July, 2003.

Experience:
As a graduate teaching assistant from August 2007 to May 2009, and a graduate research assistant from August 2006 to December 2009 with the school of Mechanical and Aerospace Engineering, Oklahoma State University, Stillwater, Oklahoma, U.S.A.

Professional Memberships:

Name: Fu, Boshen Date of Degree: December, 2009

Institution: Oklahoma State University Location: Stillwater, Oklahoma

Title of Study: SIMULATION OF MICROSTRUCTURAL EVOLUTION OF CROSS-LINKED TEMPLATED SILICA-AEROGELS UNDER COMPRESSION

Pages in Study: 48 Candidate for the Degree of Master of Science

Major Field: Mechanical Engineering

Scope and Method of Study:

The evolution of a cross-linked templated aerogel mesostructure under compression was simulated using the Material Point Method (MPM) on a model generated from X-ray nano-computed tomographic image. The aerogel mesostructure is that identified in acid-catalyzed surfactant template materials, which after cross-linking with polyurea, demonstrate very high compressive yield strengths and energy absorption capabilities. In MPM each voxel information in an X-ray tomograph was converted to a material point obtained from a nano-tomography of cross-linked aerogels to generate a MPM model. A parallel version of MPM code, developed in our group, has been used to simulate the response of a cross-linked templated aerogels under compression at high strain rates. For a comparison with experimental data, a long split Hopkinson pressure bar was used to measure the stress-strain relationship of this material at high strain rates.

Findings and Conclusions:

The results from the simulations show that the MPM can effectively model cross-linked templated silica-aerogel considering its microstructure, and capture the elastic, compaction and densification behaviors of the material, and the simulation results agree reasonably well with the experimental data. Simulations also indicate a nearly uniform compression at all three stages of deformation in the aerogel, consistent with experimental observations. Simulations were also conducted to indentify functions of ultra-thin polymer coating and the effect of density or porosity. Models with different porosities indicate that the skeletal wall thickness of both the silica particles and the polymer coating affect the local stress distribution, which in turn could induce different mechanical response under compression. MPM simulations show that the stress-strain behavior of cross-linked templated aerogels under compression follows a power law relation with bulk density.

ADVISER'S APPROVAL: Dr. Hongbing Lu